

$O(N)$ Algorithms in TBMD Simulations of the Electronic Structure of Carbon Nanotubes

G. Dereli

*Department of Physics, Middle East Technical University, 06531 Ankara, Turkey**

C. Özdoğan

Department of Computer Engineering, Çankaya University, 06530 Ankara, Turkey †

(Dated: November 11, 2018)

The $O(N)$ and parallelization techniques have been successfully applied in tight-binding MD simulations of SWNT's of various chirality. The accuracy of the $O(N)$ description is found to be enhanced by the use of basis functions of neighboring atoms (buffer). The importance of buffer size in evaluating the simulation time, total energy and force values together with electronic temperature has been shown. Finally, through the local density of state results, the metallic and semiconducting behavior of (10×10) armchair and (17×0) zig zag SWNT's, respectively, has been demonstrated.

PACS numbers: 73.22.-f, 71.20.Tx, 71.15.Pd, 71.15.Nc

I. INTRODUCTION

The carbon nanotubes are playing a major role in the design of next generation nanoelectronic and nanoelectromechanical devices due to their novel mechanical and electronic properties¹. The conductivity behavior of single walled carbon nanotubes (SWNT) is mostly determined by the chirality of the tubes. Depending on its chirality, a SWNT could be a conductor, semiconductor, or insulator. It is now widely known that the conductivity of the tubes may also change due to the presence of defects as well as radial deformations². Tight binding calculations have shown that deformations such as uniaxial compressive/tensile or torsional will also modify the band gap of the nanotubes and under such deformations SWNT undergo conducting-semiconducting-insulator transitions^{3,4}. Real space algorithms has been successfully used to perform the *ab initio* electronic structure calculations in the literature^{5–8}. The main objective of this paper is the use of $O(N)$ parallel tight binding molecular dynamics method in studying the electronic structure of SWNT's with diameters going upto 2nm. We applied the $O(N)$ and parallelization techniques in particular to (10×10) and (17×0) SWNT's.

The tight binding theory (TB) has been established as a good compromise between *ab initio* simulations and model-potential ones, bridging the gap between them, either as far as the overall numerical efficiency and/or as far as the accuracy were concerned. Tight Binding Molecular Dynamics (TBMD) is a computational tool designed to run finite-temperature MD simulations within the semi-empirical tight-binding scheme^{9,10}. This technique can be used to simulate material systems at different conditions of temperature, pressure, etc., including materials at extreme thermodynamical conditions. The electronic structure of the simulated system can be calculated by a TB Hamiltonian so that the quantum mechanical many-body nature of interatomic forces is naturally taken into account. The traditional TB solves the

Schrödinger equation by direct matrix diagonalization, which results in cubic scaling with respect to the number of atoms ($O(N^3)$). The $O(N)$ methods, on the other hand, make the approximation that only the local environment contributes to the bonding and hence band energy of each atom. In this case the run time would be in linear scaling with respect to the number of atoms. Moreover, $O(N)$ schemes can be efficiently parallelized through the use of message passing libraries. The message passing libraries such as PVM and MPI are making the simulations possible on clusters of computers. We applied these two techniques ($O(N)$ and parallelization) successfully to the SWNT simulations on a cluster of eight PC's. Details of the computational study can be found in our previous work^{11,12}.

II. THE METHOD

Traditional TB solves the Schrödinger equation in the reciprocal space by direct matrix diagonalization, which results in cubic scaling with respect to the number of atoms. The $O(N)$ methods on the other hand, solve for the band energy in real space and make the approximation that only the local environment contributes to the bonding, and hence band energy, of each atom. All the $O(N)$ methods in which the properties of the whole system are computed (such as the charge distribution, the total energy or the forces on all atoms), provide necessarily approximations to the exact solution of the effective one-electron Hamiltonian. These approximations are based on physical assumptions, which are generally connected to the above mentioned locality or nearsightedness principle in one way or another. Most of the implementations of the $O(N)$ procedure have been developed for the orthogonal tight-binding Hamiltonian. The $O(N)$ techniques may be roughly grouped into two categories: variational methods and moment-based methods. There are two types of variational methods: the density

matrix methods and localized orbital methods. There is also a variety of moment methods. The O(N) scaling, in these approaches, arises from the decay and/or truncation of these respective quantities¹³⁻¹⁵. In our work, we adopted a divide and conquer approach (DAC) first proposed by Yang¹⁶⁻¹⁷ as a linear-scaling method used to carry out quantum calculations. The basic strategy of this method is as follows: divide a large system into many subsystems, determine the electron density of each subsystem separately, and sum the corresponding contributions from all subsystems to obtain solely from the electron density¹⁸. Each subsystem is described by a set of local basis functions, instead of the entire set of atomic orbitals. The accuracy of the description is enhanced by the use of basis functions of neighboring atoms. These neighboring atoms are called the *buffer*. Here the form of the Schrödinger's equation of the buffer will be as in Ref.¹¹. The eigenvalues and vectors are found by diagonalizing the Hamiltonian matrices for each subsystem. Let \mathcal{N} be the number of atoms in the buffer region while N the number of atoms in a subsystem and $NCell$ the number of subsystems. A subsystem will be labeled by α . P^i shows the projection of the i 'th electron and $O^i \equiv f((\mathcal{E}_i - \mu)/k_B T)$ the occupation. n will be the total number of atoms in the system, $\mathcal{N}\mathcal{N}$ the number of atoms in the buffer region that are in the interaction distance (cutoff). Thus we write

$$P^i = \sum_{j=1}^{4N} |H(j, i)|^2 \quad (1)$$

where $H(j, i)$ is the ji^{th} eigenvector after diagonalization scheme and

$$O^i = \frac{2}{1 + f((\mathcal{E}_i - \mu)/k_B T)}. \quad (2)$$

Then

$$\rho_\alpha^i \equiv P^i * O^i = \frac{2}{1 + f((\mathcal{E}_i - \mu)/k_B T)} * \sum_{j=1}^{4N} |H(j, i)|^2 \quad (3)$$

and the subsystem density

$$\rho_\alpha = \sum_{i=1}^{4N} \rho_\alpha^i. \quad (4)$$

The trace

$$trace = \sum_{\alpha=1}^{NCell} \rho_\alpha \quad (5)$$

must be equal to number of electrons in the system so that the error

$$error = trace - 4 * n. \quad (6)$$

In the above expressions, $f(x) = 1/(1 + exp(x))$ is the Fermi function, μ is the chemical potential for the electrons, k_B is the Boltzmann constant, and T is the temperature of the electrons in degrees Kelvin. In case the

error exceeds the accuracy needed within the desired electron temperature, the chemical potential is recalculated from

$$\mu_{new} = \frac{-error}{d\rho} + \mu \quad (7)$$

where

$$d\rho = \sum_{\alpha=1}^{NCell} \sum_{i=1}^{4N} [(O^i * P^i) * (1 - O^i)/k_B T]. \quad (8)$$

This procedure is repeated until the desired level of accuracy is reached. The final value for the chemical potential is identified as the Fermi energy level of the system.

The band structure energy of the system is calculated as

$$E_{bs} = \sum_{\alpha=1}^{NCell} ebstot_\alpha \quad (9)$$

where $ebstot_\alpha$ shows the contribution of a subsystem to the band structure energy of the system:

$$ebstot_\alpha = \sum_{j=1}^{4N} \left[\left(\sum_{i=j+1}^{4N} 2 * density_\alpha(i, j) * \mathcal{H}(i, j) \right) + density_\alpha(i, i) * \mathcal{H}(i, i) \right] \quad (10)$$

where

$$density_\alpha(k, j) = \sum_{j=1}^{4N} \left[\left(\sum_{k=j}^{4N} \sum_{i=1}^{4N} H(j, i) * H(k, i) * O^i \right) + \left(\sum_{k=4N+1}^{4N} \sum_{i=1}^{4N} 0.5 * H(j, i) * H(k, i) * O^i \right) \right] \quad (11)$$

and $\mathcal{H}(i, j)$ is the ji^{th} element of the Hamiltonian matrix of the subsystem.

The next step is to find the forces that each atom experiences arising from the electronic structure, i.e. in the x-direction:

$$f_{x_{j=1...n}} = \sum_{\alpha=1}^{NCell} \sum_{i=1}^{\mathcal{N}} f_{x_i}^\alpha \quad (12)$$

where

$$f_{x_i}^\alpha = \sum_{j=1}^{\mathcal{N}\mathcal{N}} \sum_{im=1}^4 \sum_{jm=1}^4 density_\alpha(4(i-1) + im, 4(j-1) + jm) * Force(im, jm) \quad (13)$$

and $Force(im, jm)$ has the same form as in Ref.¹¹. Total energy of the system has the form,

$$E_{tot} = E_{bs} + E_{rep} \quad (14)$$

where E_{rep} has the same form also as in Ref.¹¹. The energetics and forces are now calculated and then molecular dynamics scheme is applied and this procedure is continued until structural stability is sustained.

III. RESULTS AND DISCUSSION

We applied the $O(N)$ and parallelization techniques in particular to (10×10) and (17×0) SWNT's. Obviously the results obtained with $O(N)$ algorithm must be consistent with $O(N^3)$ results for the same SWNT. Buffer size and the electronic temperature are the important $O(N)$ parameters that affects the results. We produced the Fermi-Dirac distribution, local density of states and energetics for the above types of SWNT's. Through these, it is possible to distinguish between the metallic and semi-conducting behavior of SWNT's depending on their chiralities.

The buffer size is an important parameter in the $O(N)$ simulations. Each subsystem has its own buffer region so that its own small sized Hamiltonian matrix. After diagonalizing this Hamiltonian matrix, the eigenvalues and eigenvectors are obtained. The next step is to obtain all these informations for all subsystems and then calculate the overall system property; chemical potential. This parameter gives us the value for Fermi energy level. Then, the forces that each atom experiences and the contribution of each subsystem to band structure energy of the system are calculated. All these procedures are repeated through each MD time step. The results obtained with $O(N)$ algorithm must be consistent with $O(N^3)$ results for the same system. To ensure this, the value for the buffer size parameter must be investigated.

Another important parameter in the simulation is the cuboidal box size. We took the cube size equal to the distance between the layers in the tube so that each cube has equal amount of atoms. This also provides the same number of interacting neighbor atoms (buffer) for each subsystem. The PBC is applied in the z -direction only. Hence, the system behaves as infinitely long tube. In Fig. 1, it is seen that the difference with $O(N^3)$ total energy result for 18 layers and 24 layers are exactly same, since PBC works well. We have chosen 20 layers for both (10×10) and (17×0) tube structures for the rest of our study.

Buffer atoms are selected using a distance criterion, R_b . That is, if an atom is within a distance R_b of a subsystem, this atom will be included as buffer atom for that subsystem. The diagonalization for a subsystem is performed with atomic basis functions of the subsystem atoms and buffer atoms, and the computational effort scales as N_α^3 , where N_α is the number of basis functions in the α subsystem and its buffer region. After diagonalization, the resulting eigenvalues and eigenvectors give us necessary information for local Density of States (IDOS) and for force expressions to evaluate the next MD iteration.

In Fig. 1, the effect of the buffer size on the total energy within the given constraints such as boxsize, electronic temperature is given. It is seen that the effect of the buffer size on the $O(N)$ TBMD is very important. For the 10×10 SWNT difference with $O(N^3)$ TBMD result (error) decreases when the buffer size is increased; then reaches to desired accuracy and fluctuates around this

value. Buffer size is important in evaluating the simulation time, energy and force values. Such as, if the buffer size is chosen a higher value than necessary, it will affect the simulation time in cubic manner since the Hamiltonian matrix is constructed with respect to the number of interacting atoms in the buffer region. On the other hand, if this parameter is chosen a low value then it will not be able to produce the correct energy and force values. In Figs. 2 and 3, the effect of the buffer size on the $O(N)$ TBMD for the (10×10) and (17×0) tube structures together with the effect of the electronic temperature are also given. From Fig. 2 the buffer size for (10×10) tube is chosen as 4.9 \AA and for (17×0) tube it is 5.7 \AA (see Figure 3). It is important to keep the buffer size parameter as small as possible and at the same time, it must be able to produce the same values with the $O(N^3)$ TBMD results. The buffer size for (17×0) tube converges to desired accuracy much later than (10×10) tube. This results in much longer simulation time.

In the Figs. 2 and 3, the effect of the buffer size together with the varying electronic temperatures (from $k_B T = 0.000001 \text{ eV}$ ($\approx 0.012 \text{ K}$) to $k_B T = 0.1 \text{ eV}$ ($\approx 1200 \text{ K}$)) on the $O(N)$ TBMD total energy value for the (10×10) and (17×0) tube structures are also given. It is seen that when the buffer size value is small, electronic temperature has a slight effect on the energy value. These values are the static results without performing simulation. The effect of the electronic temperature may be impressive during the simulation, when the forces between the atoms become dynamic. Therefore during simulations, it is safe to choose the electronic temperature as room temperature.

Next the effect of the electronic temperature on the total energy is investigated. The energetics for the pristine (10×10) tube with different electronic temperature values $k_B T = 0.025 \text{ eV}$ ($\approx 300 \text{ K}$) and $k_B T = 0.05 \text{ eV}$ ($\approx 600 \text{ K}$) are studied. Results are given in the Fig. 4. The upper graph is for the room temperature and the lower is the twice of the room temperature. Having an equal average energy value both graphs show similar behavior. They fluctuate around almost the same value. This is reasonable because they both simulate the same system with different electronic temperatures. The pattern at the above graph is more dense than the lower one. This is because of the hotter electrons in the system.

In order to observe the effect of electronic temperature on the Fermi-Dirac Distribution of the pristine (10×10) and (17×0) tubes with different electronic temperature values $k_B T = 0.01 \text{ eV}$ ($\approx 120 \text{ K}$) and $k_B T = 0.1 \text{ eV}$ ($\approx 1200 \text{ K}$) are studied. Results are given in the Figs. 5 and 6. The upper graphs in the figures are at 120 K while the lower ones are at 1200 K . It is observed that as the electronic temperature is increased the graphs are broadening. Since less electronic state is populated at the low electronic temperature condition there is no widening for the upper graphs as expected.

The density of states is obtained from the general for-

mula,

$$g(\mathcal{E}) = \frac{dN(\mathcal{E})}{d\mathcal{E}} = \frac{N(\mathcal{E} + \epsilon) - N(\mathcal{E})}{\epsilon} \quad (15)$$

where N is the number of electrons in the system and equal to,

$$N(E) = \sum_{i=1}^{NCell} \sum_{j=1}^{4N} \frac{2}{1 + f((E - \mathcal{E}_i)/k_B T)} * \sum_{j=1}^{4N} |H(j, i)|^2 \quad (16)$$

In the Eq. 15, the statement is that; if there is a change in the slope this gives us the information about the existence of populated electronic state. The criteria is the change in the slope for the Figs. 7 – 10.

In the Figs. 7 – 10, the IDOS graphs for the pristine (10×10) and (17×0) tubes for different electronic temperature values $k_B T = 0.1 \text{ eV}$ ($\approx 1200 \text{ K}$), $k_B T = 0.05 \text{ eV}$ ($\approx 600 \text{ K}$) and $k_B T = 0.025 \text{ eV}$ ($\approx 300 \text{ K}$); respectively are given. In the Figs. 7 and 9, only a selected range for IDOS are given to better understanding of the behavior of electronic states near the Fermi–Energy level for the tube structures (10×10) and (17×0) , respectively. The other figures, namely 8 and 10, give the same information but in the full range. It is seen that when the electronic temperature is increased the graphs begin to be smoother since higher amount of electronic states are populated. But, the peaks at and around the Fermi energy level are at the same positions for different electronic temperatures as expected.

The Fermi energy level values are very similar (around 3.7 eV) for both tube structures. Although they have different chirality this is expected because two tubes have the same radii. The formula for the DOS gives the electronic state population for the different energy values. It is found that the (10×10) tube has metallic behavior since it has states around Fermi energy level and a wide band gap but on the other hand the (17×0) tube has semiconducting behavior since it has no states around Fermi energy level and small band gap as expected.

We have also calculated the band gap values for (10×10) and (17×0) tubes as 2.01 eV and 0.53 eV ; respectively. In the literature^{19–24}, the proposed model values are calculated by the formulas $2\gamma_0 a_{c-c}/d$ and $6\gamma_0 a_{c-c}/d$ (where $\gamma_0 = 2.5 - 2.7 \text{ eV}$, $a_{c-c} = 0.142 \text{ nm}$, and d for diameter in (nm)) for semiconducting and metallic tubes, respectively. A theoretical value for γ_0 of 2.5 eV has been estimated by²⁵ using a first–principles local density approximation (LDA) to calculate the band structure of armchair carbon nanotube. As it is discussed in²² this

type of calculations give 10–20% smaller value for armchair nanotubes. The band gap values for the (10×10) and (17×0) Carbon Nanotubes using this model are $1.62 - 1.75 \text{ eV}$ and $0.54 - 0.58$; respectively. Our $O(N)$ TBMD algorithm gives good energy band gap result for the (17×0) tube. For the (10×10) armchair tube the model value is lower than our calculated value. On the other hand, the behaviors of the local density of states graphs are (see Figs. 7–10) as expected. For the 10×10 tube (metallic behavior), band gap is wide and there are states populated around Fermi energy level and for the (17×0) tube (semiconducting behavior), band gap is narrow and no states around Fermi energy level as expected.

IV. CONCLUSION

In this study, the details of $O(N)$ TBMD algorithm is given. It is described that how a system is divided into many subsystems and how their contributions give overall system properties (such as charge density, band structure energy) by using nearsightedness principle. This principle uses the approximation that only the local environment contributes to the bonding of each atom. This gives us the opportunity for linear scaling. The main problem in the traditional TB is the increasing system size. When the system size increases (N), the time to diagonalize the constructed Hamiltonian matrix becomes in the order of N^3 . The $O(N)$ algorithms overcome this bottleneck and the behavior has a linear scaling. It is shown in Ref.¹¹ that our $O(N)$ algorithm scales linearly for increasing system size.

To conclude, our methodology is able to produce the physical properties such as Fermi-Dirac Distribution, local Density of States and energetics for the Carbon Nanotubes. The structural stability under extreme conditions such as uniaxial strain will be studied separately.

Acknowledgments

We thank Dr. Tahir Çağm (CALTECH) for discussions and his help with $O(N)$ algorithms during his TOKTEN/UNISTAR visit. The research reported here is supported by TÜBİTAK (The Scientific and Technical Research Council of Turkey) through the project TBAG-1877 and by the Middle East Technical University through the project AFP-2000-07-02-11.

* Electronic address: gdereli@metu.edu.tr

† Electronic address: ozdogan@cankaya.edu.tr

¹ R. Saito, G. Dresselhaus, and M. S. Dresselhaus, *Physical Properties of Carbon Nanotubes*, (Imperial College Press, London, 1998).

² M. B. Nardelli, J. Bernholc, Phys. Rev. **B60**, 16338 (1999).

³ L. Yang, M. P. Anantram, J. Han, J. P. Lu, Phys. Rev. **B60**, 13874 (1999).

⁴ L. Yang, J. Han, Phys. Rev. Lett. **85**, 154 (2000).

⁵ M. B. Nardelli, Phys. Rev. **B60**, 7828 (1999).

- ⁶ J. L. Fattebert, J. Bernholc, Phys. Rev. **B62**, 1713 (2000).
- ⁷ L. Liu, C. S. Jayanthi, M. Tang, S. Y. Wu, T. W. Tomblor, C. Zhou, L. Alexseyev, J. Kong, H. Dai, Phys. Rev. Lett. **84**, 4950 (2000).
- ⁸ T. Ozaki, K. Terakura, Phys. rev. **B64**, 195126 (2001).
- ⁹ L. Colombo, Comp. Mat. Scie. **12**, 278 (1998).
- ¹⁰ P. Turchi, A. Gonis, L. Colombo (Editors), *Tight- Binding Approach to Computational Material Science*, in: Mat. Res. Symp. Proc. 491, Material research Society, Warrendal, 1998.
- ¹¹ C. Özdoğan, G. Dereli, and T. Çağın, Comp. Phys. Comm. **in print** (2002).
- ¹² C. Özdoğan, unpublished Ph. D. thesis, Middle East Technical University, 2002
- ¹³ P. Ordejon, Comput. Mater. Sci. **12**, 157 (1998).
- ¹⁴ C. S. Jayanthi, S. Y. Wu, J. Cocks, N. S. Luo, Z. L. Xie, M. Menon and G. Yang, Phys. Rev. B **57**, 3799 (1998).
- ¹⁵ D. R. Bowler, M. Aoki, C. M. Goringe, A. P. Horsfield and D. G. Pettifor, Modelling Simul. Mater. Sci. Eng. **5**, 199 (1997).
- ¹⁶ W. Yang, Phys. Rev. Lett. **66**, 1438 (1991).
- ¹⁷ T. Zhu, W. Pan and W. Yang, Phys. Rev. B **53**, 12713 (1996).
- ¹⁸ T. Lee, J. P. Lewis and W. Yang, Comput. Mater. Sci. **12**, 259 (1998).
- ¹⁹ J. W. G. Wildöer, L. C. Venema, A. G. Rinzler, R. E. Smalley, C. Dekker, Nature **391**, 59 (1998).
- ²⁰ T. W. Odom, J. Huang, P. Kim and C. M. Lieber, Nature **391**, 62 (1998).
- ²¹ T. Hertel and G. Moos, Phys. Rev. Lett. **84**, 5002 (2000).
- ²² L. C. Venema, V. Meunier, Ph. Lambin, and C. Dekker, Phys. Rev. B **61**, 2991 (2000).
- ²³ J.-C. Charlier, and Ph. Lambin, Phys. Rev. B **57**, R15037 (1998).
- ²⁴ M. Ouyang, J. Huang, C. L. Cheung and C. M. Lieber, Science **292**, 702 (2001).
- ²⁵ J. Mintmire and C. White, Appl. Phys. A: Mater. Sci. Process. **67**, 65 (1998).

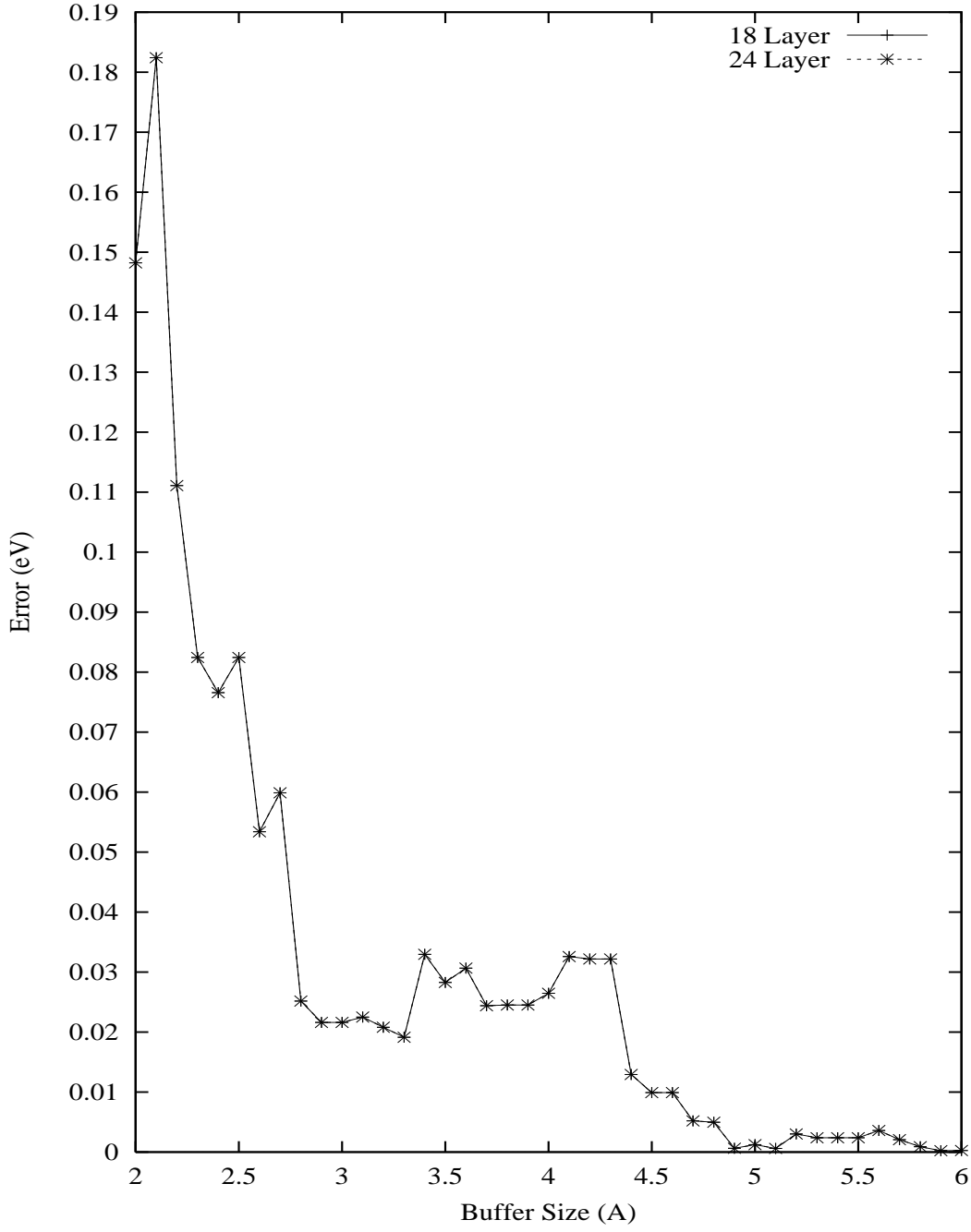


FIG. 1: The difference of $O(N^3)$ total energy result (-8.350497775) with $O(N)$ total energy result for the variation of $O(N)$ parameter (Buffer Size) for the 24 Layers and 18 Layers 10x10 Tube with box size is equal to 1.229 Å , the electronic temperature is $k_B T = 0.005$ eV.

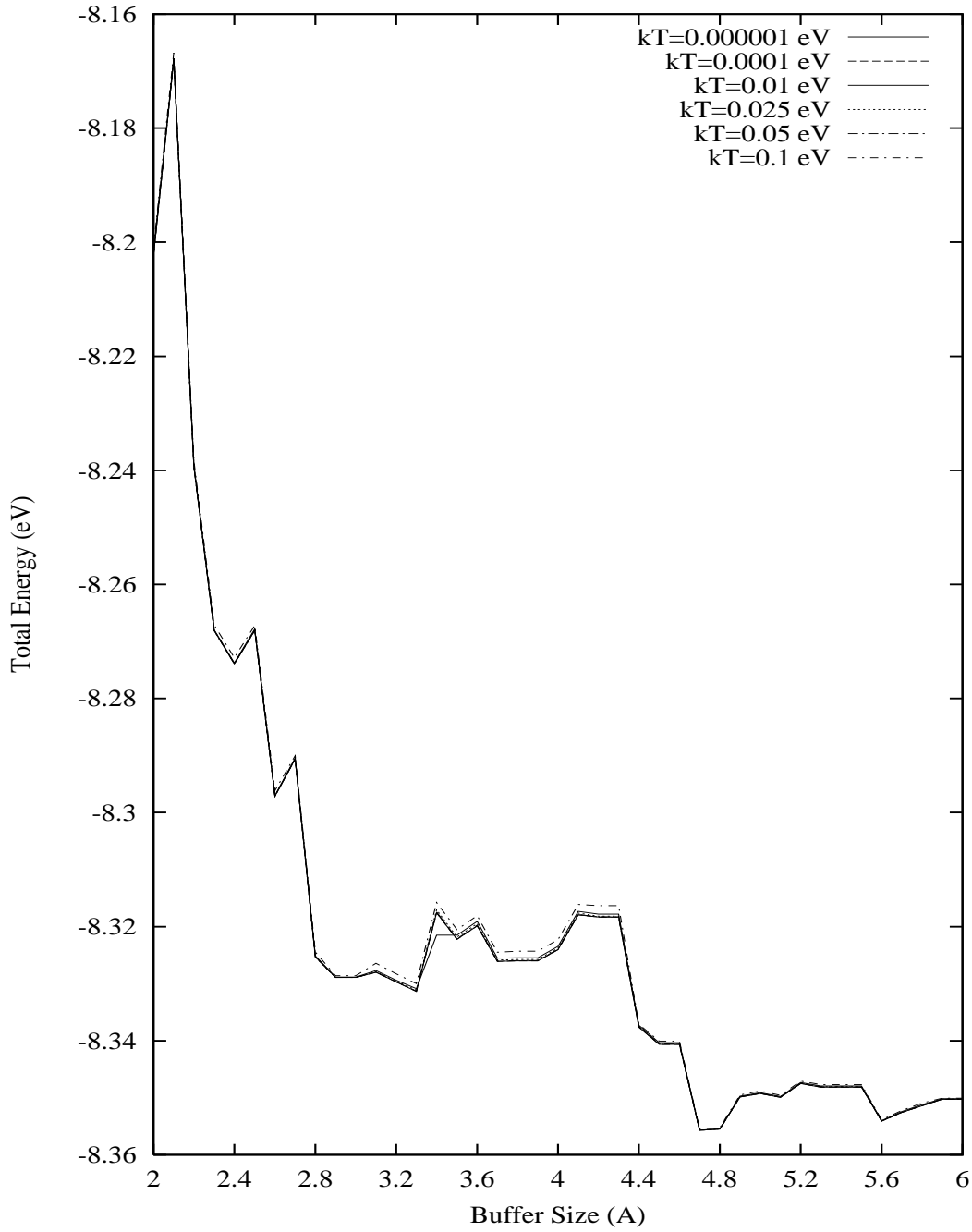


FIG. 2: The effect of Buffer Size for the Total Energy value for the tube structure 10x10, with different electronic temperature values, respectively.

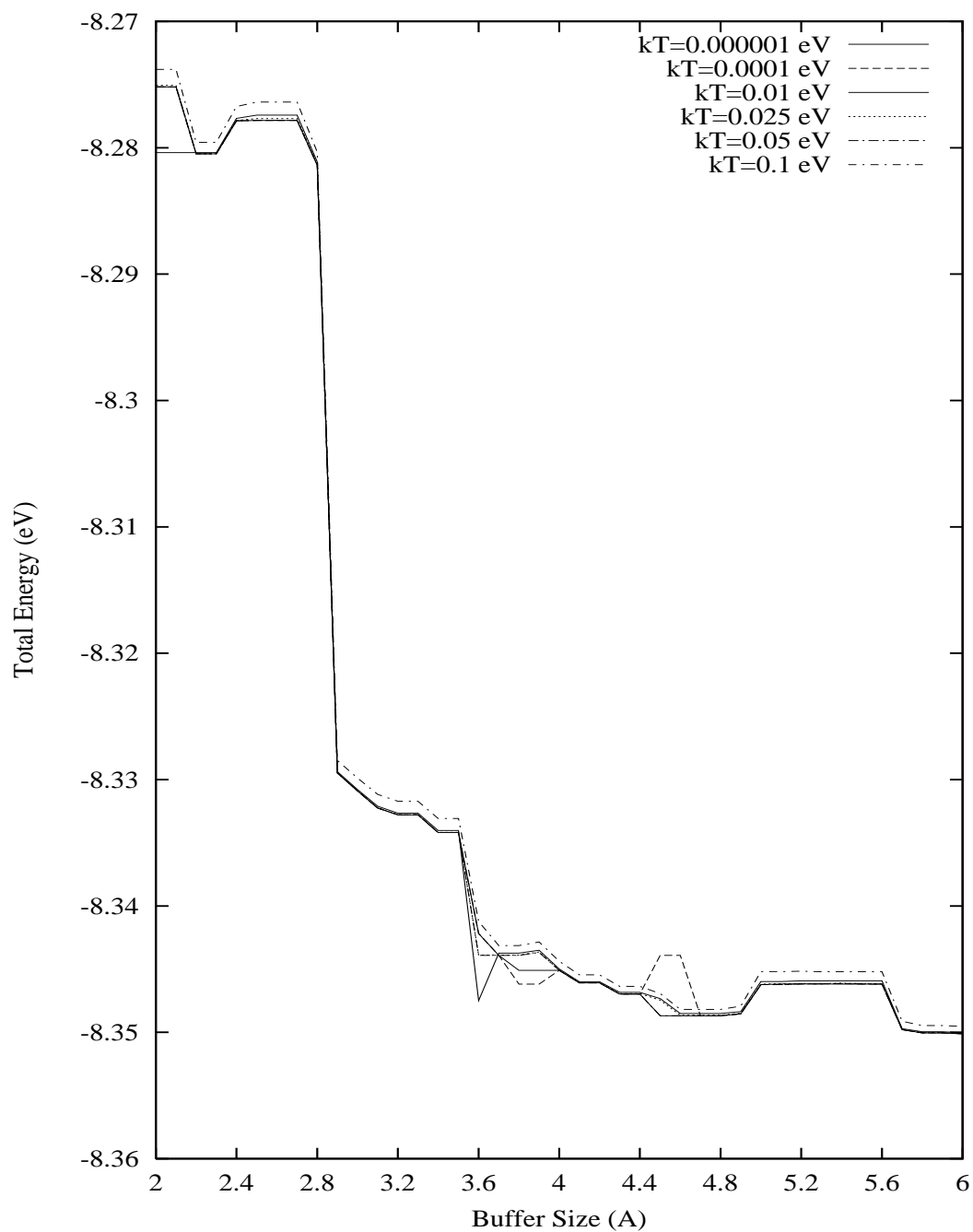


FIG. 3: The effect of Buffer Size for the Total Energy value for the tube structure 17x0, with different electronic temperature values, respectively.

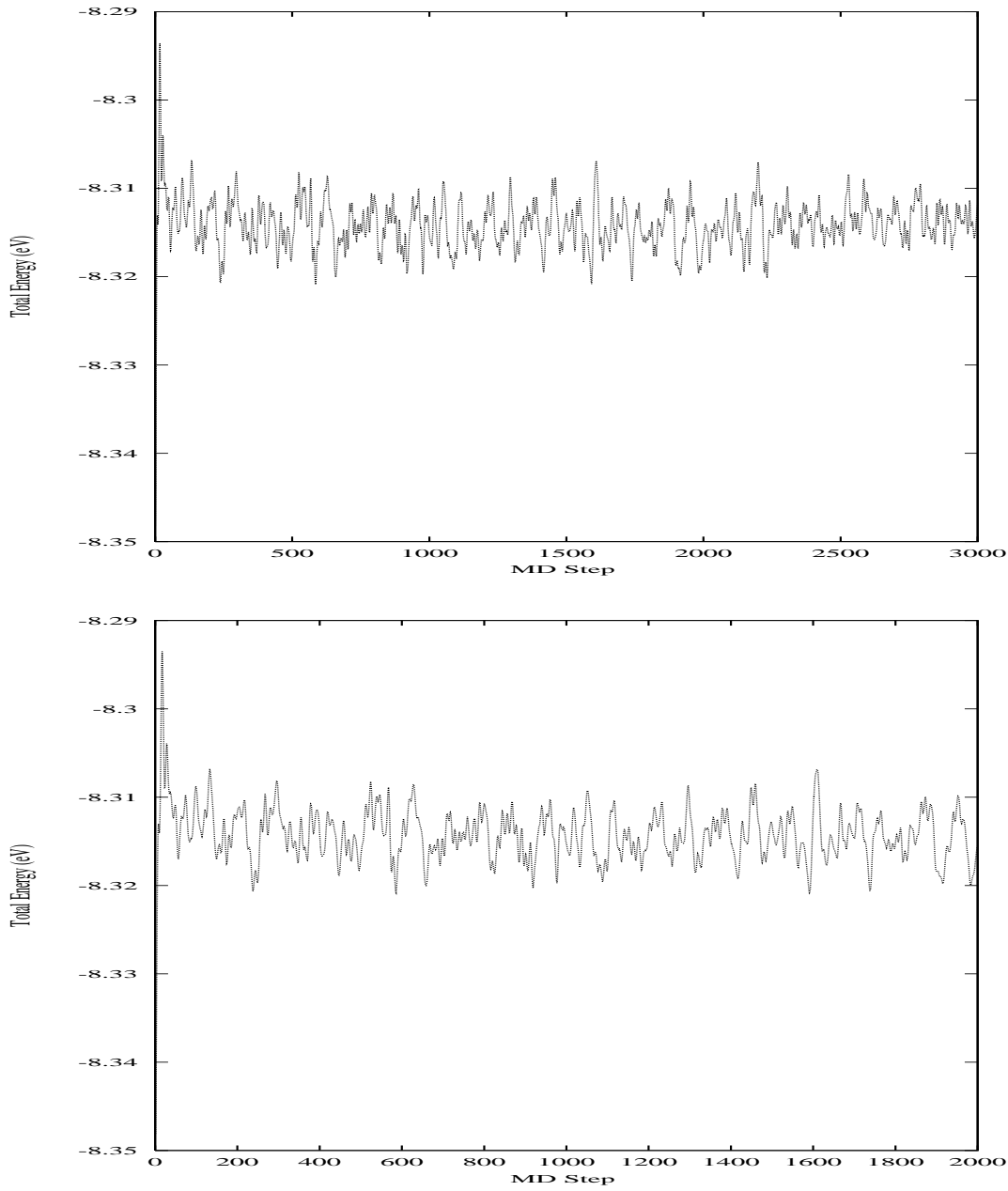


FIG. 4: The effect of electronic temperature on the total energy (Tube 10x10 no strain $T=300$ K) for the values $k_B T = 0.025$ eV and $k_B T = 0.05$ eV, respectively.

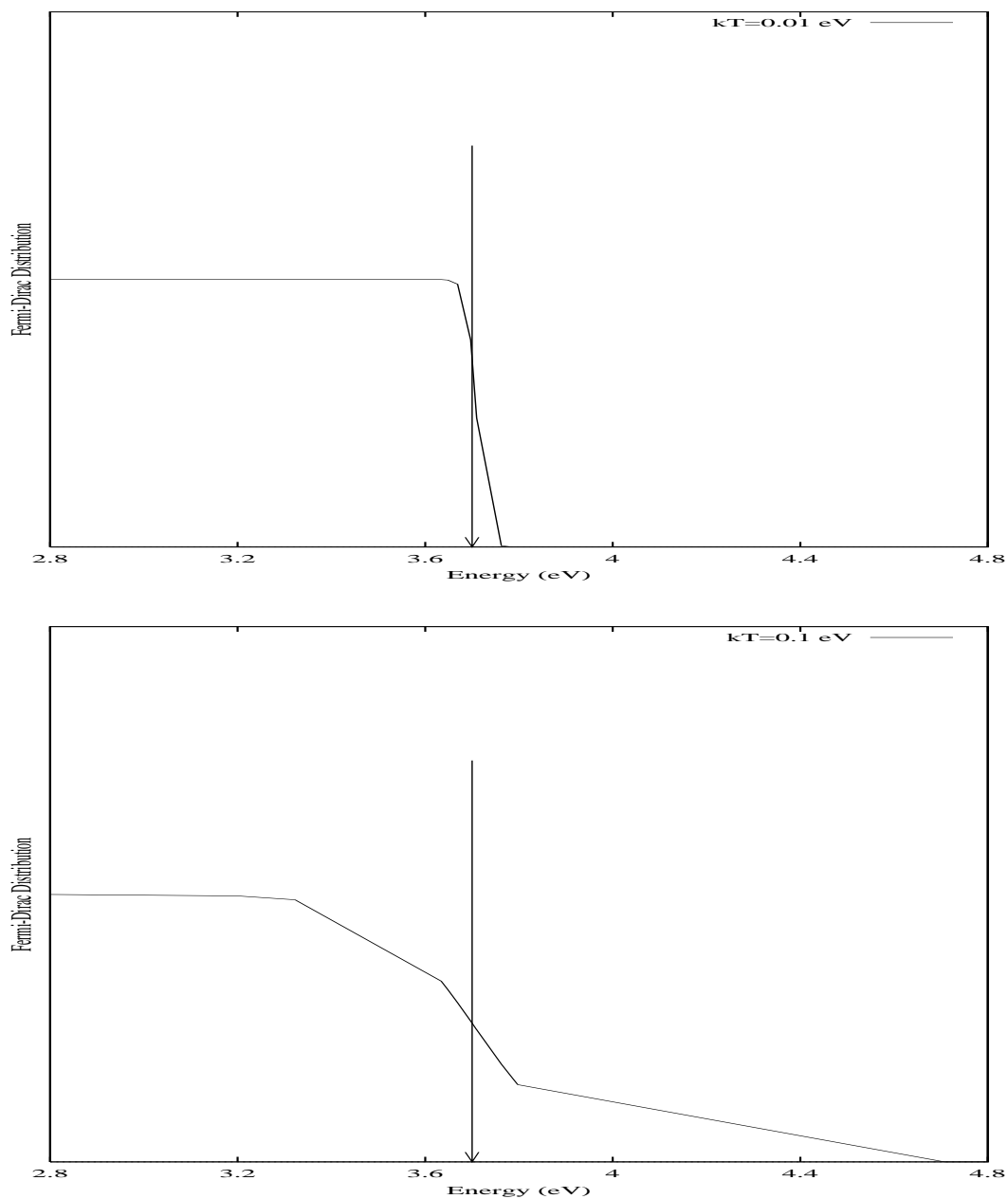


FIG. 5: Fermi-Dirac Distribution Function vs Energy for various electronic temperatures for the Tube Structure 10x10.

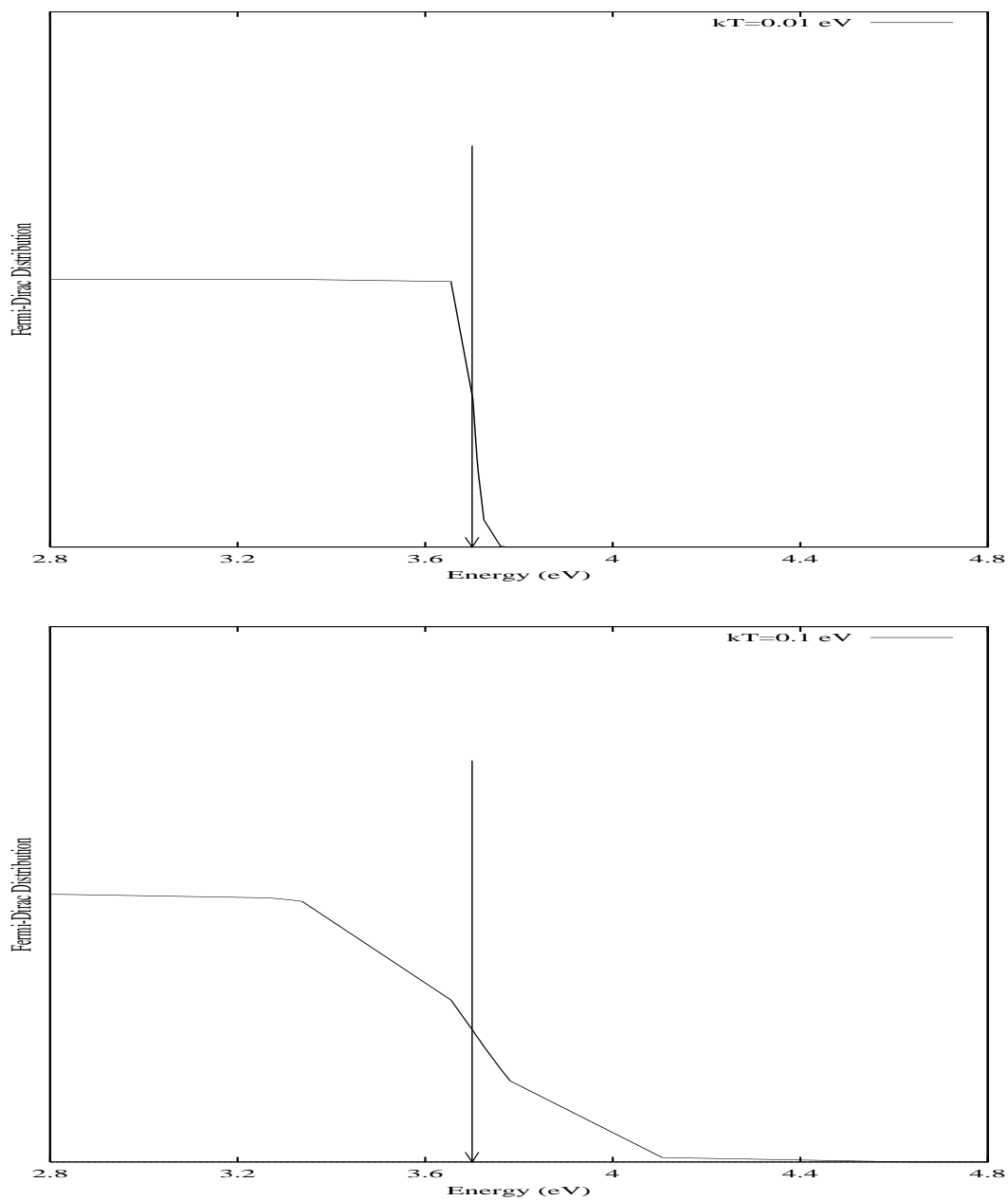


FIG. 6: Fermi-Dirac Distribution Function vs Energy for various electronic temperatures for the Tube Structure 17x0.

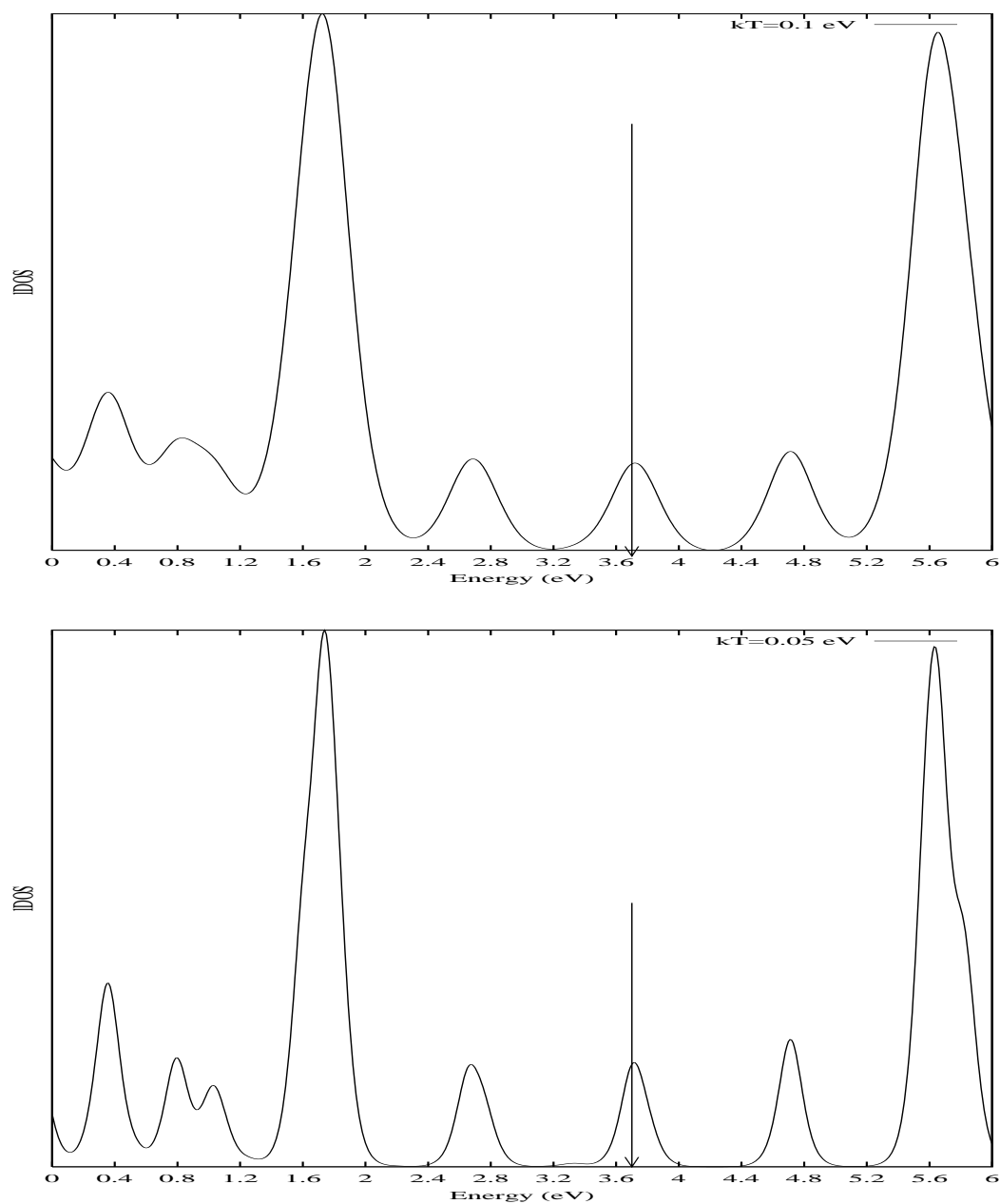


FIG. 7: Local DOS vs Energy for different electronic temperatures for the Tube Structure 10x10..

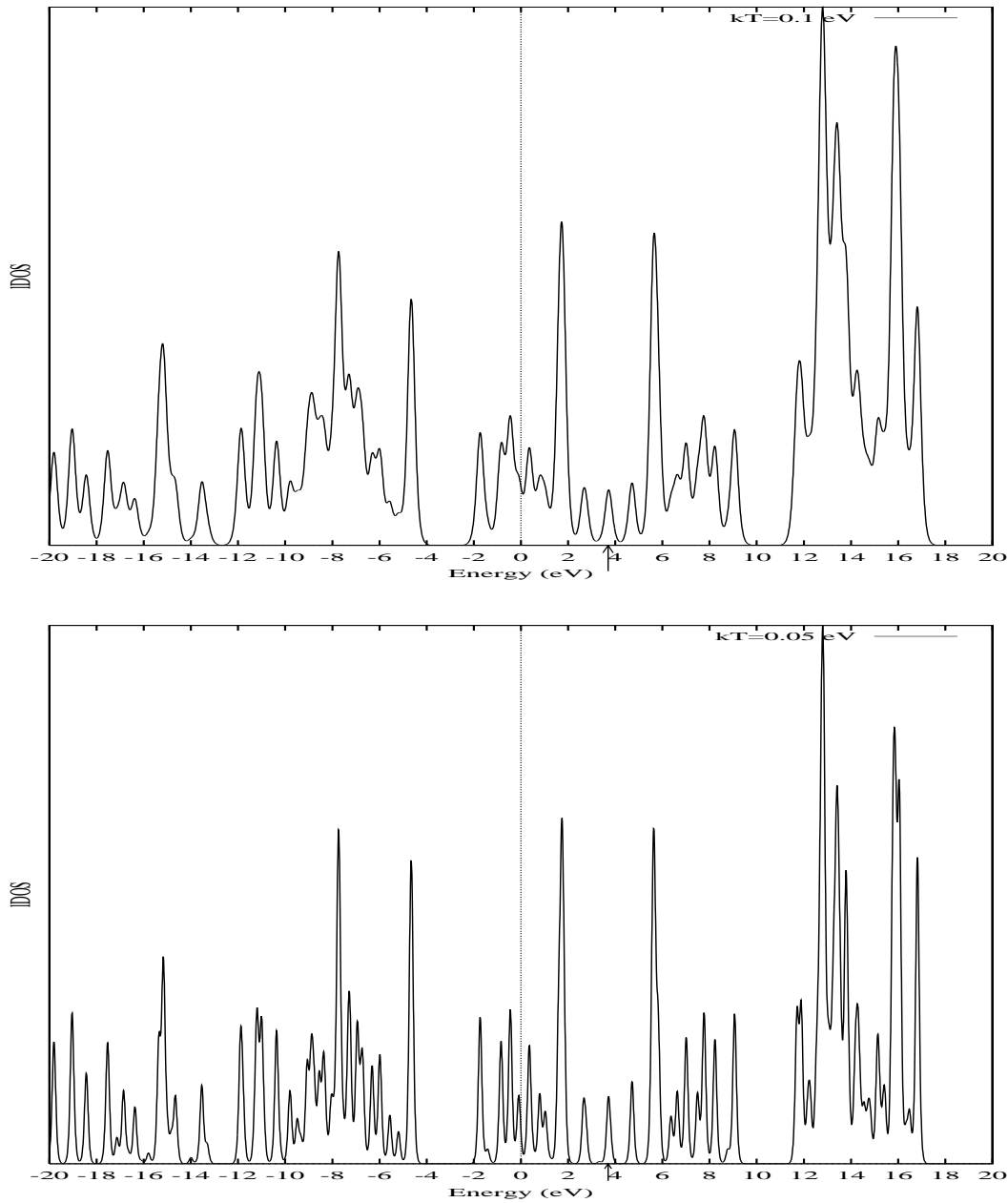


FIG. 8: Local DOS vs Energy for different electronic temperatures for the Tube Structure 10x10

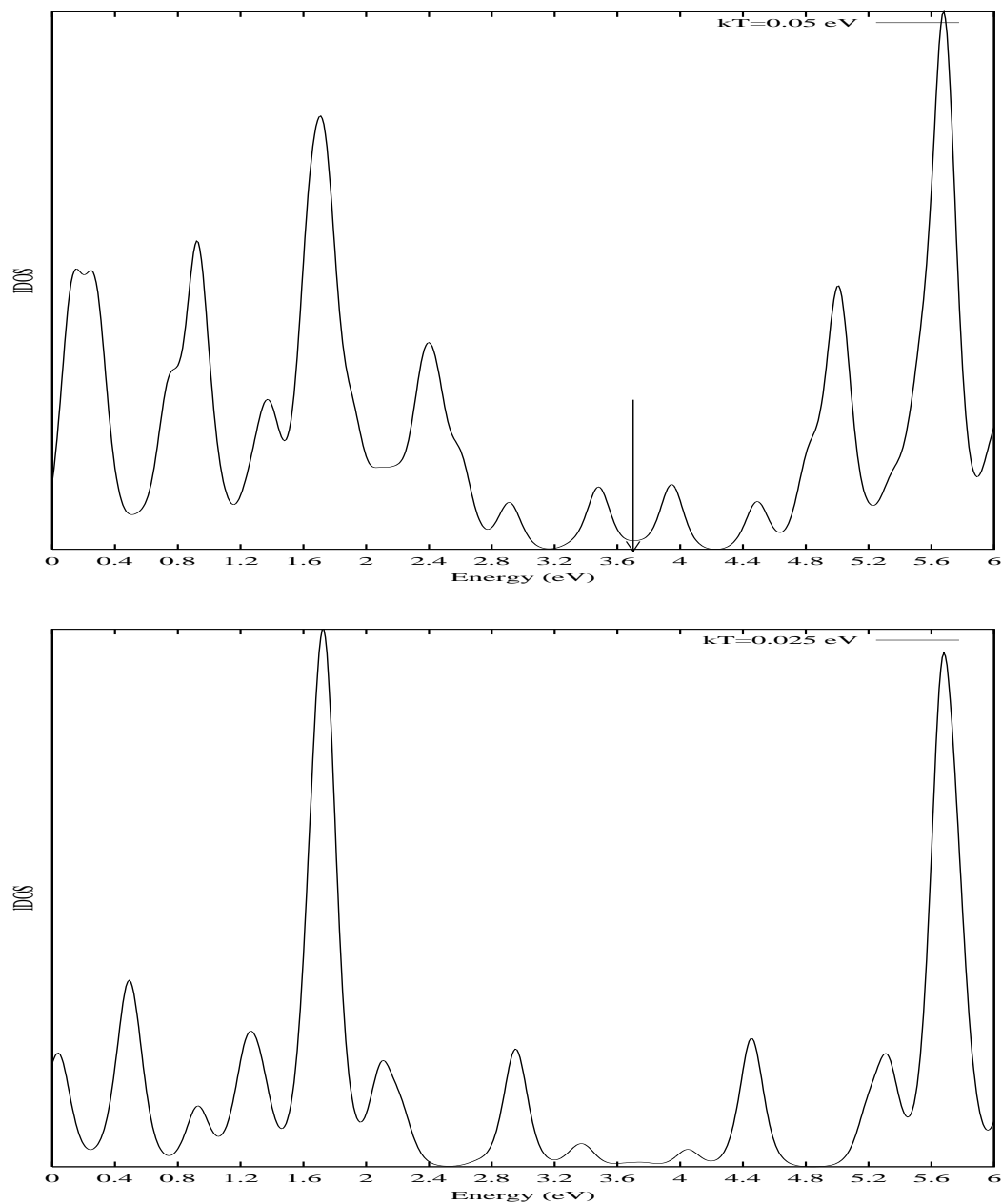


FIG. 9: Local DOS vs Energy for different electronic temperatures for the Tube Structure 17x0.

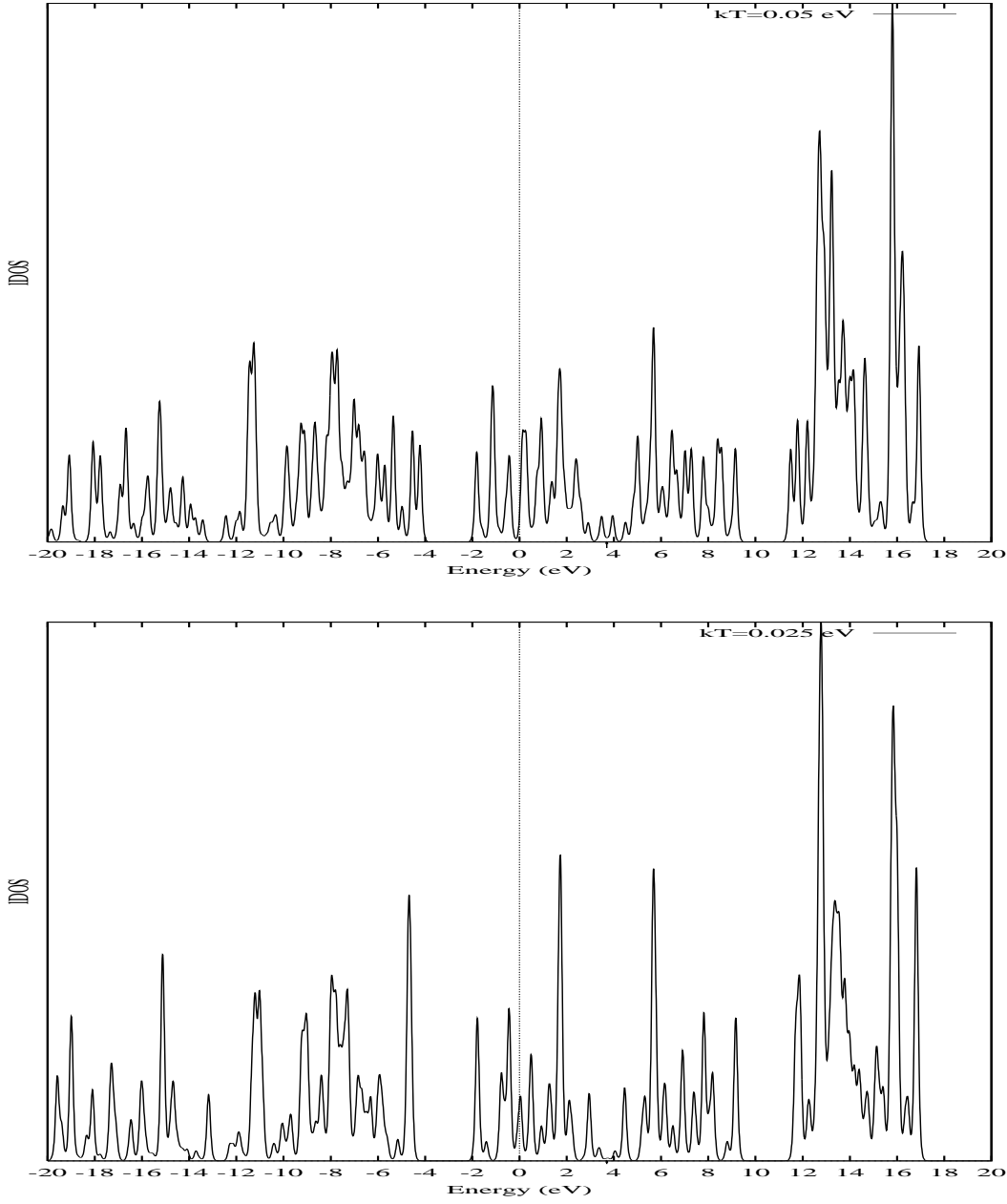


FIG. 10: Local DOS vs Energy for different electronic temperatures for the Tube Structure 17x0.